AIP | Review of Scientific Instruments

# A 32-channel photon counting module with embedded auto/cross-correlators for real-time parallel fluorescence correlation spectroscopy

S. Gong, I. Labanca, I. Rech, and M. Ghioni

Citation: Review of Scientific Instruments **85**, 103101 (2014); doi: 10.1063/1.4896695
View online: http://dx.doi.org/10.1063/1.4896695
View Table of Contents: http://scitation.aip.org/content/aip/journal/rsi/85/10?ver=pdfcov
Published by the AIP Publishing

**Articles you may be interested in**

8-channel acquisition system for time-correlated single-photon counting
Rev. Sci. Instrum. **84**, 064705 (2013); 10.1063/1.4811377

Optimum drift velocity for single molecule fluorescence bursts in micro/nano-fluidic channels
Appl. Phys. Lett. **101**, 043120 (2012); 10.1063/1.4739471

Log-normal distribution of single molecule fluorescence bursts in micro/nano-fluidic channels
Appl. Phys. Lett. **99**, 143121 (2011); 10.1063/1.3648118

Selective excitation of tryptophan fluorescence decay in proteins using a subnanosecond 295 nm light-emitting diode and time-correlated single-photon counting
Appl. Phys. Lett. **86**, 261911 (2005); 10.1063/1.1984088

Continuous real-time measurement of fluorescence lifetimes
Rev. Sci. Instrum. **73**, 3122 (2002); 10.1063/1.1488676

AIP | Chaos
CALL FOR APPLICANTS
Seeking new Editor-in-Chief

This article is copyrighted as indicated in the article. Reuse of AIP content is subject to the terms at: http://scitationnew.aip.org/termsconditions. Downloaded to IP: 131.175.132.142 On: Fri, 03 Oct 2014 14:36:06

# A 32-channel photon counting module with embedded auto/cross-correlators for real-time parallel fluorescence correlation spectroscopy

S. Gong, I. Labanca, I. Rech, and M. Ghioni
*Dipartimento di Elettronica, Informazione e Bioingegneria, Politecnico di Milano, Piazza Leonardo da Vinci 32, 20133 Milano, Italy*

(Received 30 June 2014; accepted 11 September 2014; published online 3 October 2014)

Fluorescence correlation spectroscopy (FCS) is a well-established technique to study binding interactions or the diffusion of fluorescently labeled biomolecules *in vitro* and *in vivo*. Fast FCS experiments require parallel data acquisition and analysis which can be achieved by exploiting a multi-channel Single Photon Avalanche Diode (SPAD) array and a corresponding multi-input correlator. This paper reports a 32-channel FPGA based correlator able to perform 32 auto/cross-correlations simultaneously over a lag-time ranging from 10 ns up to 150 ms. The correlator is included in a 32 × 1 SPAD array module, providing a compact and flexible instrument for high throughput FCS experiments. However, some inherent features of SPAD arrays, namely afterpulsing and optical crosstalk effects, may introduce distortions in the measurement of auto- and cross-correlation functions. We investigated these limitations to assess their impact on the module and evaluate possible workarounds.
© *2014 AIP Publishing LLC*. [http://dx.doi.org/10.1063/1.4896695]

## I. INTRODUCTION

Fluorescence Correlation Spectroscopy (FCS)[1–4] is widely used for measuring the dynamics of fluorescently labeled molecules in solution as well as inside living cells. FCS is commonly implemented by using a confocal microscope to detect the fluctuations of fluorescence intensity arising from changes in the number of molecules diffusing through a small (∼femtoliter) observation volume. The autocorrelation function (ACF) of fluorescence intensity fluctuations ($\delta I(t) = I(t) - \langle I \rangle$) can yield physical as well as photochemical information (molecule size and concentration, blinking or binding/unbinding rates) about the diffusing molecules. To monitor the fluorescence fluctuations, FCS measurements need to be performed at nanomolar concentrations with typical acquisition times on the order of a few seconds to several minutes. However, faster acquisitions of FCS data are desirable in two cases: in high-content screening approaches, many molecules on reaction at different locations require simultaneous interrogation; also when observing fast evolving dynamic systems, diffusion parameters change as a function of time. Parallel FCS acquisition is thus developed, with the help of multi-pixel detectors and multi-spot excitation generation technique,[5] which maps each excitation spot onto every target pixel of the detector. Furthermore, simultaneous data acquisition and processing is needed, demanding for multi-input high efficiency correlators.

Hardware photon correlators have been traditionally employed for real-time calculation of correlation functions over a certain dynamic range. Since in typical FCS measurements the correlation function spans over several decades of lag times, linear channel spacing is impractical and the multiple-$\tau$ algorithm (MTA) is used.[6,7] Real-time, multiple-$\tau$ correlators were formerly implemented on custom high-speed digital signal-processing hardware, either application-specific integrated circuits (ASICs)[8–10] or, lately, field-programmable gate arrays (FPGAs).[11–16] Nowadays, FPGAs are manufactured in 45 nm CMOS processes and have reached integration densities that allow cost efficient implementation of even complex and resource intensive DSP algorithms. They offer lower non-recurring engineering costs and faster time to market than more customized approaches such as full-custom VLSI or ASIC design. Remarkable FPGA implementations of multichannel real-time correlators have been recently demonstrated. For example, Jakob *et al.*[17] reported a 32-channel parallel correlator covering a dynamic range of $\sim 10^{13}$ (from 5 ns to nearly 1 h), whereas Bucholz *et al.*[18] reported a massively parallel autocorrelator array having 1024-channel although with a narrower dynamic range (from 10 $\mu$s to 1 s).[5]

In this paper we present a FPGA-based multichannel correlator featuring a lag-time ranging from 10 ns up to 150 ms, which can perform real-time computation of 32 autocorrelation or cross-correlation functions simultaneously. This correlator has been specifically designed to work in combination with a 32 × 1 Single Photon Avalanche Diode (SPAD) array[19] developed in our lab. Both the SPAD array and the multichannel correlator are housed in a user friendly photon counting module that can be easily interfaced to a PC via USB connection. This compact and efficient data detection and analysis unit can greatly simplify the FCS experimental setup.

The application of monolithic SPAD arrays in parallel FCS experiments has been recently investigated by different research groups. Preliminary FCS results obtained using a liquid crystal on silicon spatial light modulator (LCOS-SLM) and a CMOS 1024 pixel SPAD array were reported by Colyer *et al.*[20,21] in solution and by Kloster-Landsberg *et al.*[22] in living cells. Bucholz *et al.* used a CMOS 32 × 32 SPAD array[23] in combination with a custom selective plane illumination microscope (SPIM)[24] and a 1024-channel FPGA correlator[18] for

 © 2014 AIP Publishing LLC

This article is copyrighted as indicated in the article. Reuse of AIP content is subject to the terms at: http://scitationnew.aip.org/termsconditions. Downloaded to IP: 131.175.132.142 On: Fri, 03 Oct 2014 14:36:06

imaging FCS in 3D samples.[25] The quest for better detector sensitivity and larger pixel size led to the development of custom SPAD arrays,[26,27] which were successfully exploited in multispot FCS measurements by Colyer *et al.*[5,21]

The use of a single SPAD array in FCS experiments has the disadvantage that SPAD afterpulsing dominates the short time scale behavior of the ACFs, preventing one from studying sub-microsecond dynamic phenomena.[28,29] A standard workaround in single spot FCS is to use a Hanbury Brown and Twiss (HBT) configuration, using two SPADs, each collecting 50% of the emitted signal split by a beam-splitter cube and computing the cross-correlation function (CCF) of the two detector signals.[3] A multispot HBT configuration using two SPAD arrays would be a straightforward extension of this strategy, although perfect alignment of the two array detectors would present a new challenge. Alternatively, a dual-view system[30] can be used to split a 16-spot emission pattern and to focus and align the 16 spots on two halves of the SPAD array. CCF would then be performed between two SPAD pixels belonging to the two halves of the 32-pixel array (i.e., 1-17, 2-18. . . 16-32). This approach has already been exploited by Ingargiola *et al.*[31] in single-molecule Förster resonance energy transfer (smFRET) experiments. However, such approach must face another potential shortcoming of monolithic SPAD arrays, which arises from the photon emission from an avalanching junction. When an avalanche is triggered, photons are emitted by intraband relaxation of hot-carriers crossing the junction.[32] These emitted photons can trigger an avalanche in neighboring pixels, thus causing optical crosstalk among the pixels. Unless negligible, optical crosstalk would introduce spurious artifacts in the CCF. In this paper we present a thorough characterization of both afterpulsing and optical crosstalk effects in order to assess their impact on our detection system.

This paper is organized as follows: Sec. II describes the design and implementation of the FPGA-based 32-channel correlator. Section III briefly reviews the geometry of the 32-pixel SPAD array and illustrates the development of the associated photon counting module. Section IV will then report the experimental measurements aimed at assessing the impact of afterpulsing and optical crosstalk on the performance of the multichannel correlation system. We conclude this article with a brief overview of future prospects for the field.

## II. 32-CHANNEL FPGA-BASED CORRELATOR DESIGN

### A. Theoretical background

In FCS the fluctuation of the fluorescence intensity is characterized by its normalized autocorrelation function:

$$g(\tau) = \frac{\langle I(t) \cdot I(t+\tau)\rangle}{\langle I(t)\rangle^2}, \tag{1}$$

where $I(t)$ is the fluorescence intensity at time $t$, $\langle I(t)\rangle$ is the time average of the signal, and $\tau$ is the correlation (or lag) time.

Since output signals from SPADs are discrete pulses indicating incident photons or dark counts, triangular averaging is used for $I(t)$, which turns to be the number of detected events n(i) measured within a sampling time interval $\Delta t$ centered on time $t_i$. Thereby the normalized ACF estimator is defined by

$$\hat{g}(k) = \frac{\langle n(i) \cdot n(i+k)\rangle}{\langle n(i)\rangle^2}, \tag{2}$$

where

$$\langle n(i) \cdot n(i+k)\rangle = \frac{1}{M-k} \sum_{i=1}^{i=M-k} n(i) \cdot n(i+k), \tag{3}$$

$k \in \mathbb{N}$ is the discrete lag time in units of $\Delta t$ (i.e., $\tau = k\ \Delta t$) and $M$ is the total number of time bins of size $\Delta t$ measured during the experiment.

In Eq. (2), standard (asymmetric) normalization of the ACF is applied, which may not be able to remove completely the statistical noise. Instead, a symmetric normalization[33] can remove not only the baseline error but also the linear error contribution for lag times much longer than coherence time.[34] The symmetrically normalized ACF estimator can be written as

$$\hat{g}(k) = \frac{\langle n(i) \cdot n(i+k)\rangle}{\langle n(i)\rangle\ \langle n(i+k)\rangle}, \tag{4}$$

where

$$\begin{aligned} \langle n(i)\rangle &= \frac{1}{M-k} \sum_{i=1}^{i=M-k} n(i), \quad \text{and} \\ \langle n(i+k)\rangle &= \frac{1}{M-k} \sum_{i=1+k}^{i=M} n(i). \end{aligned} \tag{5}$$

In the case of cross-correlation, with $n_X(i)$ and $n_Y(i)$ being the number of counts of two separate channels, the symmetrically normalized CCF estimator is defined by

$$\hat{g}(k) = \frac{\langle n_X(i) \cdot n_Y(i+k)\rangle}{\langle n_X(i)\rangle \langle n_Y(i+k)\rangle}, \tag{6}$$

where

$$\begin{aligned} \langle n_X(i)\rangle &= \frac{1}{M-k} \sum_{i=1}^{i=M-k} n_X(i), \quad \text{and} \\ \langle n_Y(i+k)\rangle &= \frac{1}{M-k} \sum_{i=1+k}^{i=M} n_Y(i). \end{aligned} \tag{7}$$

In order to achieve a high dynamic range, we adopted the multi-tau algorithm.[6,7,33]

A multi-tau correlator separates the lag times into several blocks, where each block has a sampling time interval being a multiple of that of the previous block. $S$ linear correlator blocks are then chained to provide a multi-tau correlator (see Figure 1). The sampling time interval of each block can be written as

$$\Delta t_s = \Delta t_0 \cdot m^s, \tag{8}$$

where s is the index of the correlator block ($s = 0,1,\ldots, S-1$), $\Delta t_0$ is the sampling time interval of the fastest linear correlator (i.e., the one employing the minimum time bin), and the integer $m$ is the multiplication factor. Inside a correlator block the spacing of lag-times is linear; between consecutive blocks it increases by a factor of $m$. Within the sth linear correlator block the lag-times of the correlation channels are

$$\tau_s(l) = \tau_s(0) + \Delta t_s \cdot l, \tag{9}$$

This article is copyrighted as indicated in the article. Reuse of AIP content is subject to the terms at: http://scitationnew.aip.org/termsconditions. Downloaded to IP: 131.175.132.142 On: Fri, 03 Oct 2014 14:36:06

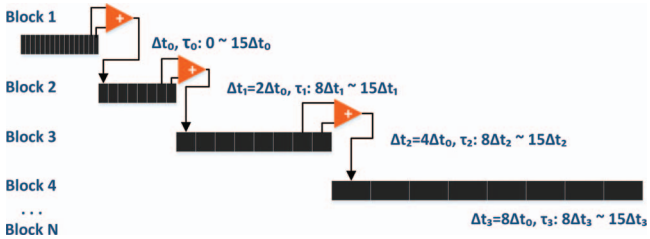


FIG. 1. Data generation unit of each block. Each block gets data by adding last two elements of the shift register of the previous block. Sampling time of each block is double of the previous one. The delay time range of each block is then $8\Delta t_n \sim 15\Delta t_n$.

where $l$ is the index of a correlation channel within the block ($l = 0,1,\ldots,p-1$), $p$ being the number of correlation channels in the sth block.

As reported in Refs. 35 and 36 certain artifacts may occur with a coarser grid due to the triangular averaging effect, but by ensuring the ratio $\alpha = p/m$ be large than 7, the distortions can be reduced to less than $10^{-3}$. In our implementation we adopted the most common setting, i.e., $m = 2$, $p = 16$. Therefore, if the shorter sampling time interval is 10 ns, with 21 blocks (176 correlation channels) we can achieve a total lag time of 150 ms, whereas in a linear correlator it would require $10^7$ correlation channels to reach the same lag time.

### B. Implementation

The goal of our design is to implement a 32-channel auto/cross-correlator inside a cost-effective, Xilinx XC6SLX150 FPGA device. A single-channel correlator featuring a lag time range spanning from 10 ns to 150 ms was already implemented in such device, resulting in a slice occupation of 12%.[37] A straightforward replication of this design to obtain a multichannel correlator is not a viable solution, since it would provide at most 8 parallel channels. To overcome this limitation, we developed a new design that makes it possible to efficiently reuse the available FPGA resources.

Each channel of the correlator was provided with two inputs, in order to easily compute auto- and cross-correlation functions. A multiplexer was used to properly distribute the SPAD-generated signals among the available inputs. As a result, the 32-channel auto/cross-correlator can receive 64 input signals and is able to compute 32 autocorrelation or cross-correlation functions simultaneously.

As stated before, a multi-tau correlator is realized by cascading several linear correlator blocks. Each block has a shift register array and computation unit, and the adjacent blocks are linked by data generation units. As shown in Figure 1, block one receives the undelayed signal stream, fills up the 16-element shift register continuously with initial sampling time $\Delta t_0$. By adding up the last two elements of block one, data are passed to block two, filling the second shift register. Thereby, the lag time range in block two turns out to be $16\Delta t_0$ to $30\Delta t_0$, with sampling time being double of that of block one. The following blocks obey the same rule. In the single-channel design,[37] we have the same algorithm to update the shift registers, but each register has a depth of 16, which actually wasted resources to store the first eight non-computed elements. So in the multichannel design, we only reserve eight elements for each shift register except the first block.

Another difference involves the computation unit, which in the single-channel design is a multiply adder implemented by the embedded DSP48A1 slices,[38] whereas for the 32-channel correlator, the number of DSP slices are no longer enough to satisfy the demanding requests. To circumvent this limitation, the different correlator channels in the same block have to share one multiply adder unit. This was achieved by resorting to the time division multiple use of a multiply adder (TDM-MA). This strategy employs one multiply adder in a certain block to sequentially compute correlation functions for several channels within one macro clock cycle $T_{ma}$. The performance rate of the multiply adder is thereby related to the micro clock $T_{mi}$, equal to $T_{ma}$ divided by the overall computation times (see Figure 2).

The macro time $T_{ma}$ starts from 10 ns for block one and doubles each subsequent block. So the blocks can be separated into three groups according to their macro clocks: fast speed group ($T_{ma} < 640$ ns, block 1 to block 6), middle speed group (640 ns $\leq T_{ma} < 2560$ ns, block 7 and block 8) and slow speed group ($T_{ma} \geq 2560$ ns, block 9 to block $S$). Fast speed blocks, limited by their high clock frequency, have to fully devote the linear correlator structures to each channel. These are the most resource consuming blocks. Middle speed blocks are able to share one multiply adder among 8 or 16 channels, whereas slow speed blocks, due to the advantage of long clock periods, allow TDM-MA for all the 32 channels (see Figure 3). Results from every multiply adder are continuously stored into one block RAM (BRAM). TDM-MA not only avoids shortage of the embedded DSP slices but, combined with BRAMs, greatly reduces occupation of the logic resources as well.

The new scheme is illustrated in Figure 4; instead of employing full correlator structure for each channel, the

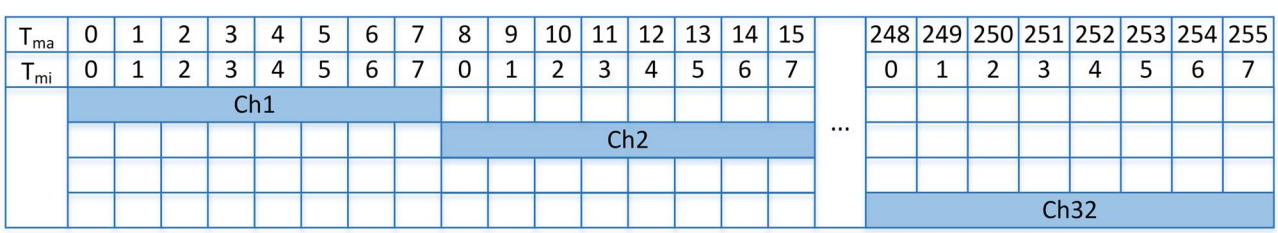


FIG. 2. Execution sequence of TDM-MA. In a block with macro clock period $T_{ma} \geq 2560$ ns, employing one multiply adder allows to complete correlation calculation of 32 channels, each channel containing 8 lag times. The corresponding micro clock $T_{mi}$ is equal to $T_{ma}/256$. The upper frequency limit of the multiply adder is set to be 100 MHz.

This article is copyrighted as indicated in the article. Reuse of AIP content is subject to the terms at: http://scitationnew.aip.org/termsconditions. Downloaded to IP: 131.175.132.142 On: Fri, 03 Oct 2014 14:36:06

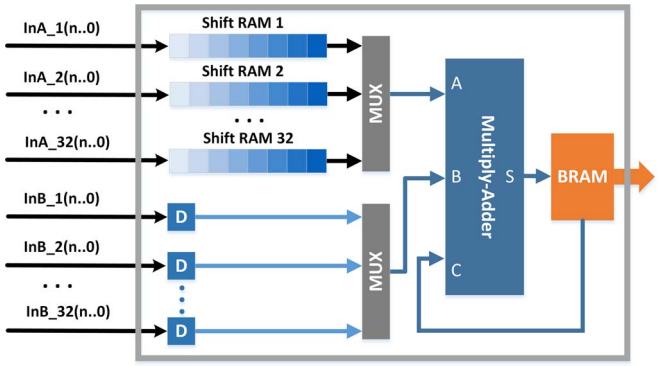


FIG. 3. Structure of TDM-MA: input data coming from the previous block of different channels are stored and shifted simultaneously inside relevant distributed RAMs. Correlation functions are computed in succession employing a multiply adder. Multiplexer is used to switch among channels. Results from the multiply adder keep updating the following BRAM.

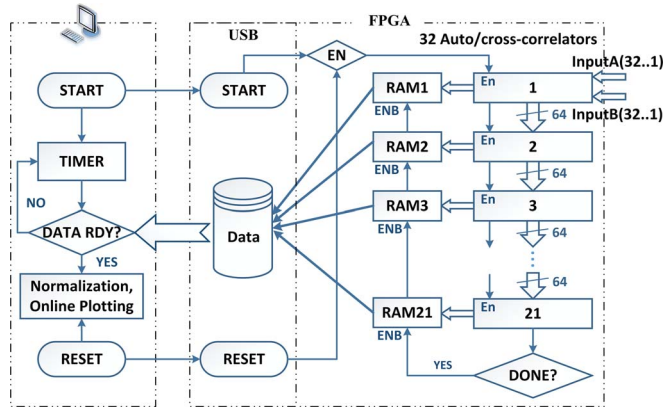


FIG. 5. Schematic diagram of the complete multichannel correlator system. The left part is the PC interface that controls the operation of the FPGA (right) and receives the results computed by the FPGA.

replication is done inside the blocks. Each block has a full set of 32 channels sharing some common structures, with data generation unit linking the following block.

A simple PC interface was designed to assign the pairing among the 64 inputs for the FPGA-based correlator, control the correlation computation, and manage data transfer, processing and visualization. Upon starting the correlation routine, a data stream containing all the auto/cross-correlation results is continuously sent to the PC from the FPGA via USB. A timer is set to wake up the interface and check if data in the USB FIFO reached the required amount. The PC interface then stores all the data in a dedicated file and carries out the normalization according to Eq. (4) or (6). Thirty two correlation functions are plotted in real time each illustrating the correlation between the two input pulses. The whole process is schematically illustrated in Figure 5.

## III. 32-CHANNEL PHOTON DETECTION MODULE

We here review the key features of the multichannel photon counting module. More details can be found in Ref. 19. The core of the system is the 32-pixel SPAD array shown in Figure 6. The array was fabricated using a custom planar silicon process described in Ref. 39. The active area diameter of each pixel is 50 $\mu$m whereas the pixel pitch is 250 $\mu$m.

The large diameter allows for an easier mechanical alignment of the detector. The relatively high ratio between pixel pitch and active area radius (10 in this array) makes it possible to reduce the amount of light collected from

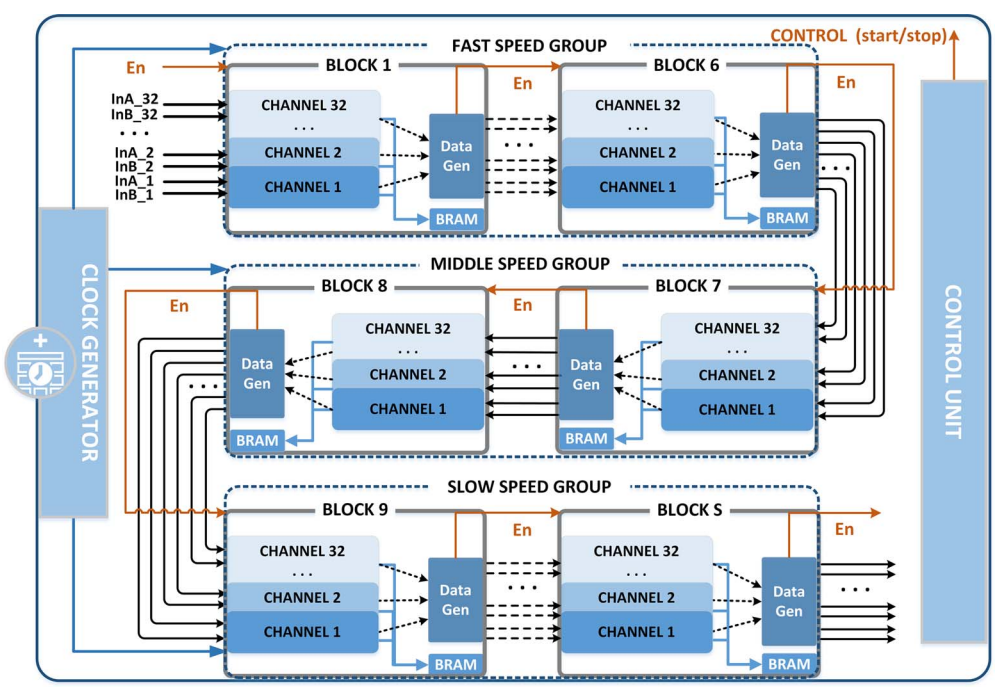


FIG. 4. Structure of 32-channel correlator. Multiple channels are built inside each block instead of simply replicating the whole single-channel correlator structure. According to different clock frequency, the blocks are separated into three groups: fast, middle speed, and slow, representing also the degree of resource sharing.

This article is copyrighted as indicated in the article. Reuse of AIP content is subject to the terms at: http://scitationnew.aip.org/termsconditions. Downloaded to IP: 131.175.132.142 On: Fri, 03 Oct 2014 14:36:06

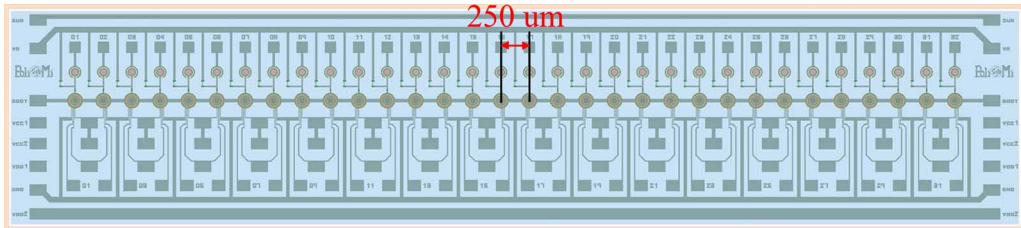


FIG. 6. Microphotograph of the 32 × 1 linear SPAD array.

nonconjugated spots.[40] Each SPAD pixel is connected to an external active quenching circuit (AQC), which quenches the SPAD avalanche and resets the initial bias condition making the device ready for detecting a new photon.[41] A monolithic 32 × 1 AQC array (iAQC) was designed and fabricated by using a highly scaled, 0.18 $\mu$m High-Voltage CMOS technology, in order to reduce area occupancy, power dissipation and dead time (see Figure 11). Extreme care was taken in the design of the connections between the SPAD and the iAQC arrays to make electrical crosstalk among channels negligible. We then developed a compact module (13.5 × 11.9 × 2.6 cm$^3$) to include the sensor and the associate electronics. The SPAD array and the iAQC chip are housed into a hermetically sealable chamber separated from the remaining part of the module.[19] Sealing in a dry atmosphere makes it possible to mount the SPAD array on a double-stage Peltier and to cool the detector down to temperatures of about −20 °C, thereby reducing the dark count rate of SPAD devices and increasing the sensitivity of the instrument. A C-mount thread at the top of the detector chamber allows for a simple and reliable connection to the single-molecule optical setup. All the electronic circuitry needed for a proper operation of the detection system is housed outside the sealed chamber. In particular a power supply board generates all the voltage levels needed both by the detectors and by the iAQC. The same board implements also a closed-loop temperature control by reading the detector's temperature (thanks to a Negative Temperature Coefficient thermistor) and by suitably driving the Peltier cooler. A second board reads the output signals from the iAQCs and assures the interfacing with the onboard FPGA (Xilinx Spartan 6, model SLX150) that performs correlations. Processed data can be exported through a USB 2.0 transceiver (the FT2232H device from FTDI Chip) by connecting the photon detection head to a PC. The FPGA firmware also provides a direct connection between the 32 photon-counting inputs and 32 output LVCMOS outputs that are fed to a 68-pin SCSI VHDCI connector. Remote control of the system is performed through a graphical user interface (GUI) developed in Visual C# language. A picture of the photon counting module is shown in Figure 7.

## IV. EXPERIMENTAL RESULTS

Several tests were made to characterize the developed system in terms of photon detection efficiency, dark count rate, afterpulsing, and optical crosstalk. Preliminary measurements were carried out by operating the SPAD array at room temperature with an excess bias voltage of 6 V. The hold-off time of the iAQC was regulated to obtain a total dead-time of 60 ns. Dead-time is the minimum recovery time required for the detector being able to detect the next photon after a previous detection event: measurement of the ACF is prevented in this time interval. In general, the sub-100 ns time region is of little interest in FCS measurements, therefore we will not consider dead-time effects further. However, the dynamic range of the correlator can be fully exploited down to the minimum lag-time by performing cross-correlation measurements as reported in Sec. IV D.

### A. Photon detection efficiency

Figure 8 shows the photon detection efficiency (PDE) of the 32 SPAD pixels measured at different wavelengths. Measurements were performed by using a standard optical

FIG. 7. Picture of 32 × 1 SPAD array module. The FPGA is placed on the bottom side of the visible printed circuit board.

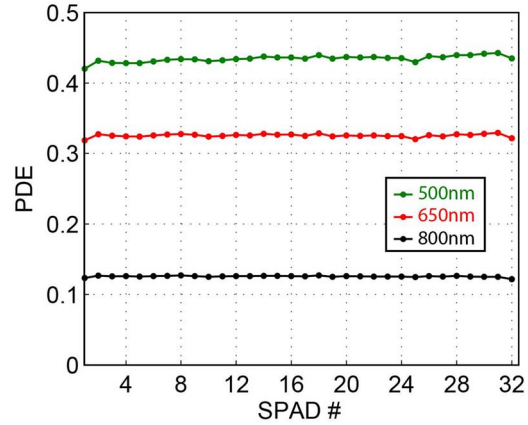


FIG. 8. Photon Detection Efficiency of the 32 SPAD pixels measured at room temperature. All devices are biased at 6 V above the breakdown level.

This article is copyrighted as indicated in the article. Reuse of AIP content is subject to the terms at: http://scitationnew.aip.org/termsconditions. Downloaded to IP: 131.175.132.142 On: Fri, 03 Oct 2014 14:36:06

including a halogen light source, a monochromator (Oriel Spectraluminator 69050), used to generate a monochromatic beam with selectable wavelength (400–1000 nm), and an integrating sphere, used to generate a uniform light beam. The light beam was attenuated by means of a neutral density filter and directed towards the detector placed at a known distance. The system was calibrated using a reference power meter whose readings are finally compared to the ones obtained by the detector under test. Experimental data show that the PDE is highly uniform over the array, with a peak-to-peak spread of only a few percent. The PDE peaks at 550 nm, where its value exceeds 45% for all the pixels of the array.

### B. Dark count rate

The dark count rate (DCR) is defined as the number of avalanche pulses per unit time that occur in the absence of incident photons. In SPAD devices operating at room temperature or below, the dark count rate is dominated by thermal generation of carriers, as well as by trap-assisted and band-to-band tunneling processes in the depletion layer.[42,43] A photon-counting measurement with time-window set to 30 s was performed to estimate the DCR. Figure 9 shows the DCR of the 32 SPADs, measured at room temperature and –10 °C respectively. It is worth noting that at room temperature 90% of the channels feature DCR < 20 kcps, and by decreasing the temperature to –10 °C, the DCR can be reduced by more than a factor of ten.

### C. Afterpulsing probability

Deep levels located at intermediate energies between mid-gap and band edge may act as carrier traps. During each avalanche pulse carriers can be trapped in these levels and subsequently released with a statistically fluctuating delay, whose mean value depends on the deep levels actually involved. The released carrier can re-trigger the avalanche, thereby generating correlated afterpulses.[41,44]

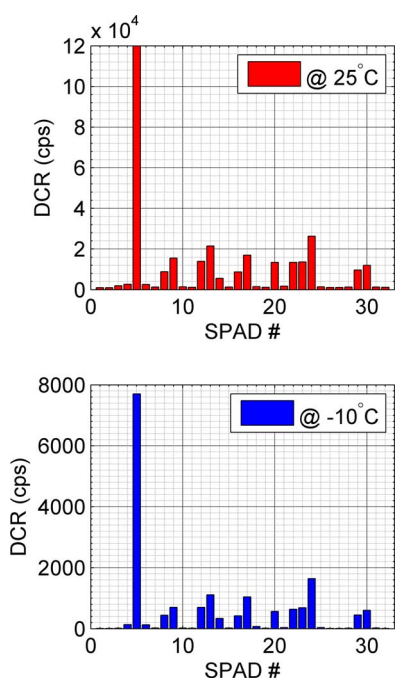


FIG. 9. DCR measured at room temperature and −10 °C respectively, with 6 V excess bias voltage. An average reduction of the DCR by a factor of 45 is observed at −10 °C.

The probability of detecting an afterpulse in the time interval between $t$ and $t + \Delta t$ after an avalanche current pulse is $P_a(t)\Delta t$, where $P_a(t)$ is the afterpulsing probability density. SPADs typically exhibit a multi-exponential afterpulsing probability density with longest decay lifetimes in the $\mu$s range:[59]

$$P_a(t) = A_1 \exp\left(-\frac{t}{\tau_1}\right) + A_2 \exp\left(-\frac{t}{\tau_2}\right) + \ldots, \qquad (10)$$

where $A_1, A_2, \ldots$ are amplitudes of the different exponential components at the end of the hold-off time, which is $t = 0$ in Eq. (7), and $\tau_1, \tau_2$ are lifetimes of carriers trapped in different levels.

Important for FCS is that afterpulsing is a secondary phenomenon that is correlated to an initial output pulse. Thus, afterpulsing becomes visible as a fast decay of the ACF at lag times comparable with the trap lifetimes. This distortion makes it often impossible to clearly distinguish between fast photophysical processes such as triplet state dynamics and detector afterpulsing.[29]

On the other hand, the distortion of the ACF can be effectively used to characterize afterpulsing in the SPAD array. This can be done simply by placing the 32-channel photon counting module in dark environment or illuminating it with source of continuous classic light, such as an incandescent lamp or an LED, and allowing the embedded autocorrelators to build up the 32 ACFs. The time needed to get satisfactory ACFs in dark conditions at room temperature is less than 1 h; by comparison, the Time Correlated Carrier Counting (TCCC)[44] technique, which is normally applied in our lab for afterpulsing characterization, requires at least 15 min to acquire the same information in a single channel, resulting in a total measurement time of more than 8 h for all the 32 channels. The measurement duration might become unbearably long if SPAD detectors are cooled down to a certain temperature, due to the reduction of the DCR. This effect is usually counteracted by deliberately increasing the environmental illumination through an uncorrelated light source. At −10 °C operating temperature, we used a LED source to increase the average count rate to about $10^4$ cps, thus making it possible to collect the 32 ACFs shown in Figure 10 in less than 30 min.

Each ACF peaks at $T = 60$ ns, which is consistent with the duration of the dead-time. The height of the ACF peak depends on the count rate in each SPAD. The reason is that the probability of detecting the afterpulse of a previously detected photon is constant, whereas the probability of detecting another photon increases with the count rate. To make the results directly comparable, the ACFs must be scaled with the count rate. It can be noticed that afterpulsing is negligible after a few $\mu$s for any SPAD pixel.

This article is copyrighted as indicated in the article. Reuse of AIP content is subject to the terms at: http://scitationnew.aip.org/termsconditions. Downloaded to IP: 131.175.132.142 On: Fri, 03 Oct 2014 14:36:06

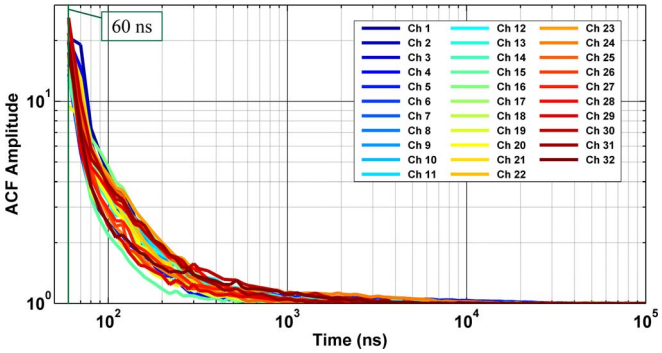


FIG. 10. Autocorrelation curves for the 32 SPAD pixels cooled down to $-10\,^{\circ}$C, operated with an average count rate of $10^4$ cps. The afterpulsing peaks occur at the end of the dead-time (60 ns). The different ACF amplitude arises from various count rate in each pixel.

The autocorrelation function is related to the afterpulsing probability density as follows:[28]

$$g(\tau) = \frac{\Delta t}{\langle i \rangle} P_a(\tau) + 1, \tag{11}$$

where $\langle i \rangle$ represents the mean count number during each dwell time, $\Delta$t. Therefore, the ratio $\langle i \rangle / \Delta t$ indicates the average count rate. Starting from Eq. (11) we can easily calculate the total afterpulsing probability, defined as

$$\varepsilon = \int_{T_d}^{+\infty} P_a(t) dt, \tag{12}$$

where $T_d$ is the dead-time.

Figure 11 shows that the total afterpulsing probability is below 2% for all of the SPAD pixels except the fifth channel which also has comparatively high dark count rate. These figures are consistent with those obtained with the TCCC technique. Moreover, by changing the environmental illumination, the overall deviation of afterpulsing probability calculated according to Eq. (12) for each pixel is smaller than 0.1% which in turn proves the computational algorithm.

As reported elsewhere, we performed comparative afterpulsing experiments in the same conditions by using a Becker and Hickl TCSPC module (BandH SPC 130).[37] The results are consistent with those obtained with our module, thus confirming the correct operation of the multichannel correlator.

### D. Optical crosstalk

Silicon p-n junctions emit photons when operated in avalanche regime. The emission probability is very low: on the average, about one photon is emitted every $10^5$ carriers crossing the junction.[32] In monolithic SPAD arrays, photons emitted from a SPAD can trigger an avalanche in another detector, thus causing optical crosstalk between the pixels of the array. The crosstalk probability increases as the distance between pixels is reduced, and therefore sets a limit to the array density. Optical barriers placed between adjacent pixels (such as deep trenches coated with metals or heavily doped diffusions) cannot completely prevent the optical crosstalk because photons can be reflected at the bottom surface of the chip, thus bypassing the optical barriers and contributing substantially to the crosstalk.[45,46]

In order to assess the impact of optical crosstalk on the 32-channel SPAD array module, we first performed cross-correlation measurements between each pair of adjacent pixels (center-to-center distance equal to 250 $\mu$m). A total of 64 CCFs were collected, which are shown in Figure 12. As expected, a spurious peak due to the optical crosstalk mechanism is observable for each SPAD pair at the very beginning of the CCFs. Once being triggered in a SPAD of the pair, the avalanche current and so the photon emission last for about 4 ns before the AQC quenches it.[47] In addition, the minimum time bin width in our correlators is 10 ns thus making cross-correlated counts to be mainly concentrated in the first two bins around $\tau = 0$ ns. A tiny and relatively broad peak is also noticed around 60 ns (a zoom of this peak is shown in the inset). This small peak is due to a combination of crosstalk and afterpulsing. There are several possible chain of events leading to the formation of this peak; for instance: (1) avalanche is triggered in SPAD "A;" after a dead-time (60 ns), (2) an afterpulse is generated in SPAD "A," and (3) SPAD "B" is triggered due to a crosstalk photon. As a consequence the pulse generated by SPAD "B" is correlated to the one generated by SPAD "A." The probability of this event is relatively low, being the product of the crosstalk and afterpulsing probabilities.

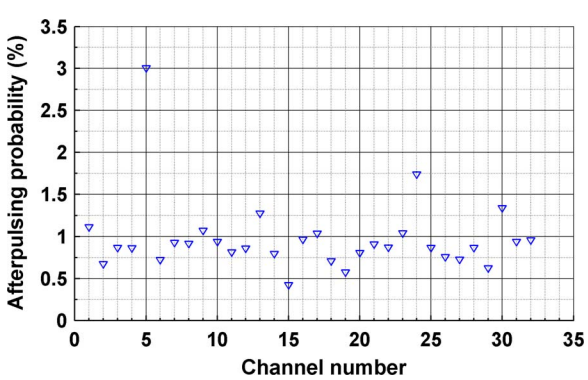


FIG. 11. Total afterpulsing probability for each pixel of the array at $-10\,^{\circ}$C. Remarkably, more than 90% of the 32 pixels have a total afterpulsing probability of less than 1.5% at $-10\,^{\circ}$C and more than 80% of them will be even lower than 1% if operated at room temperature.

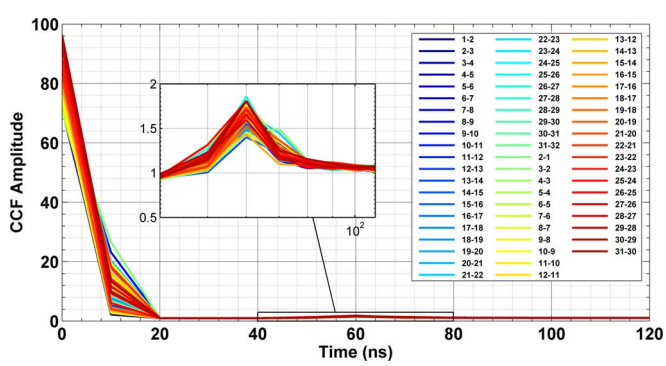


FIG. 12. Cross-correlation measurements between pairs of adjacent SPAD pixels. For each pair, a sharp peak appears at $\tau = 0$ ns due to optical crosstalk. A delayed, less intense peak is barely observable around 60 ns due to the combination of optical crosstalk and afterpulsing effects. A zoom of the delayed peaks is shown in the inset.

This article is copyrighted as indicated in the article. Reuse of AIP content is subject to the terms at: http://scitationnew.aip.org/termsconditions. Downloaded to IP: 131.175.132.142 On: Fri, 03 Oct 2014 14:36:06

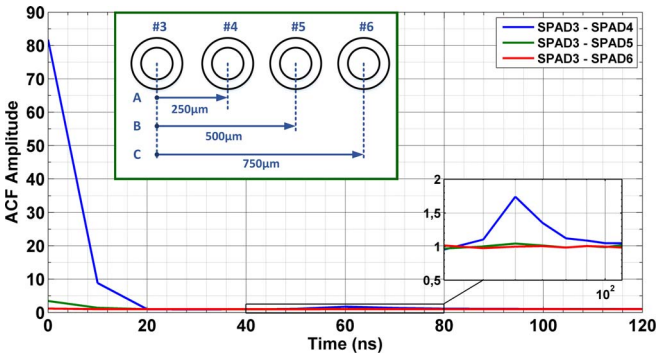


FIG. 13. Cross-correlation measurements between SPAD pixels located at three different distances (see inset). The amplitude of spurious peaks due to optical crosstalk is maximum for SPADs located at 1 pitch distance, decreasing to almost zero for SPADs located at 3 pitches distance. Crosstalk is negligible between pairs of SPADs separated by more than 3 pitches (750 $\mu$m).

We then compared cross talk effect between SPAD pixels located at different distance over the array. Figure 13 shows a collection of three CCFs between pairs of SPAD devices separated by 1 pitch, 2 pitches, and 3 pitches. Same as the adjacent pixel pairs, the peak at $\tau = 0$ ns is due to the crosstalk caused by photon emission from the avalanching pixel. The peak amplitude is maximum for SPADs located at 1 pitch distance, decreasing to almost zero for SPADs located at 3 pitches distance. Accordingly, the height of the secondary peak becomes negligible for pixel distance greater than 3 pitches as well. We verified that crosstalk is negligible between pairs of SPADs separated by more than 3 pitches (750 $\mu$m).

In conclusion, crosstalk free cross-correlation measurements can be performed by using SPAD pairs in the monolithic array, as long as they are separated by at least three pitches.

## V. CONCLUSION

We developed a multichannel FPGA-based correlator able to perform 32 parallel auto- or cross-correlations. Thanks to the multiple-$\tau$ architecture the correlator provides a large-span of lag-times, ranging from 10 ns up to 150 ms. This correlator is included in a 32 × 1 SPAD array module, providing a compact and flexible instrument for advanced FCS experiments.

Although monolithic SPAD arrays offer distinct advantages in the development of compact, high throughput FCS systems, some of their inherent features, namely afterpulsing and optical crosstalk effects may introduce distortions in the measurement of auto and cross-correlation functions. We therefore investigated these limitations to assess their impact on the module and evaluate possible workarounds. In particular, SPAD afterpulsing prevents one from studying sub-microsecond dynamic phenomena (Fig. 10). However, as demonstrated by Zhao *et al.*,[28] if the afterpulsing decays quickly and the total probability of afterpulsing is small than distortions of the ACF due to afterpulsing can be corrected by a simple mathematical treatment. The implementation of such a correction routine in our multichannel module is currently under investigation. Alternatively, a HBT configuration can be exploited, using two halves of the SPAD array, each collecting 50% of the emitted signal split by a beam-splitter cube, and computing the cross-correlation function of the two detector signals.[4] Despite the challenging alignment procedure, this configuration would completely eliminate spurious effects due to afterpulsing and dead-time, extending the true dynamic range of the correlator down to 10 ns. We demonstrated that optical crosstalk between SPAD pixels can be reduced to negligible level if the distance between the SPAD pair used for computing the CCF is higher than 750 $\mu$m. In the envisioned "dual view" configuration[31] applied to our 32-pixel SPAD array, the distance between SPAD pairs would be 4 mm (that is, 16 times the pitch) thus virtually eliminating the optical crosstalk. Moreover, a HBT configuration using a dichroic mirror instead of a beam-splitter cube to distinguish photons emitted in different spectral ranges would allow high throughput two-color fluorescence cross-correlation spectroscopy (FCCS), a powerful extension of FCS with many fundamental and biotechnological applications[48]

Future developments of the multichannel module for high throughput FCS will be mainly driven by user demands for detector performance, which naturally set requirements for the device design and fabrication technology. Work is ongoing in multiple directions to increase the pixel number, extend the spectral sensitivity and improve the photon-performance.[27]

## ACKNOWLEDGMENTS

This work was supported in part by the National Institute of General Medical Sciences of the National Institutes of Health under Awards 5R01 GM095904. The content is solely the responsibility of the authors and does not necessarily represent the official views of the National Institutes of Health. M. Ghioni discloses equity in Micro Photon Devices S.r.l. (MPD), Bolzano, Italy. No resources or personnel from MPD were involved in this work.

[1] E. L. Elson and D. Magde, "Fluorescence correlation spectroscopy. I. Conceptual basis and theory," Biopolymers **13**, 1–27 (1974).
[2] D. Magde, E. L. Elson, and W. W. Webb, "Fluorescence correlation spectroscopy. II. An experimental realization," Biopolymers **13**, 29–61 (1974).
[3] O. Krichevsky and G. Bonnet, "Fluorescence correlation spectroscopy: the technique and its applications," Rep. Prog. Phys. **65**, 251–297 (2002).
[4] E. Haustein and P. Schwille, "Fluorescence correlation spectroscopy: Novel variations of an established technique," Annu. Rev. Biophys. Biomol. Struct. **36**, 151–169 (2007).
[5] R. A. Colyer, G. Scalia, I. Rech, A. Gulinatti, M. Ghioni, S. Cova *et al.*, "High-throughput FCS using an LCOS spatial light modulator and an 8×1 SPAD array," Biomed. Opt. Exp. **1**, 1408–1431 (2010).
[6] K. Schätzel, "Correlation techniques in dynamic light scattering," Appl. Phys. B **42**, 193–213 (1987).
[7] K. Schatzel, "New concepts in correlator design," in *Institute of Physics Conference Series No. 77* (Hilger, Bristol, 1985), pp. 175–184.
[8] M. Engels, B. Hoppe, H. Meuth, and R. Peters, "A single chip 200 MHz digital correlation system for laser spectroscopy with 512 correlation channels," in *Proceedings of the 1999 IEEE International Symposium on Circuits and Systems, ISCAS'99* (IEEE, 1999), Vol. 5, pp. 160–163.
[9] B. Hoppe, H. Meuth, M. Engels, and R. Peters, "Design of digital correlation systems for low-intensity precision photon spectroscopic measurements," IEE Proc.-Circ. Dev. Syst. **48**, 267–271 (2001).
[10] M. Engels, B. Hoppe, H. Meuth, and R. Peters, "Fast digital photon correlation system with high dynamic range," in *Proceedings of 13th*

This article is copyrighted as indicated in the article. Reuse of AIP content is subject to the terms at: http://scitationnew.aip.org/termsconditions. Downloaded to IP: 131.175.132.142 On: Fri, 03 Oct 2014 14:36:06

*Annual IEEE International Conference, ASIC/SOC 2000* (IEEE, 2000), pp. 18–22.
[11]C. Jakob, A. Schwarzbacher, B. Hoppe, and R. Peters, "The development of a digital multichannel correlator system for light scattering experiments," in *Irish Signals and Systems Conference, IET* (IET, 2006), pp. 99–103.
[12]C. Jakob, A. T. Schwarzbacher, B. Hoppe, and R. Peters, "A FPGA optimised digital real-time multichannel correlator architecture," in *10th Euromicro Conference on Digital System Design Architectures, Methods and Tools, DSD* (IEEE, 2007), pp. 35–42.
[13]Y. Yang, J. Shen, W. Liu, and Y. Cheng, "Digital real-time correlator implemented by field programmable gate array," in *Congress on Image and Signal Processing, CISP '08* (IEEE, 2008), Vol. 1, pp. 149–151.
[14]W. Liu, J. Shen, and X. Sun, "Design of multiple-tau photon correlation system implemented by FPGA," in *International Conference on Embedded Software and Systems, ICESS'08* (IEEE, 2008), pp. 410–414.
[15]S. Kalinin, R. Kühnemuth, H. Vardanyan, and C. A. M. Seidel, "Note: A 4 ns hardware photon correlator based on a general-purpose field-programmable gate array development board implemented in a compact setup for fluorescence correlation spectroscopy," Rev. Sci. Instrum. **83**, 096105 (2012).
[16]G. Mocsar, B. Kreith, J. Buchholz, J. W. Krieger, J. Langowski, and G. Vamosi, "Note: Multiplexed multiple-tau auto- and cross-correlators on a single field programmable gate array," Rev. Sci. Instrum. **83**, 046101 (2012).
[17]C. Jakob, A. Schwarzbacher, B. Hoppe, and R. Peters, "A multichannel digital real-time correlator as single FPGA implementation," in *Proceedings of the 2007 15th International IEEE Conference on Digital Signal Processing (DSP 2007)* (IEEE, 2007), pp. 276–279.
[18]J. Buchholz, J. Krieger, G. Mocsár, B. Kreith, E. Charbon, G. Vámosi, U. Kebschull, and J. Langowski, "FPGA implementation of a 32×32 autocorrelator array for analysis of fast image series," Opt. Express **20**, 17767–17782 (2012).
[19]A. Cuccato, S. Antonioli, M. Crotti, I. Labanca, A. Gulinatti, I. Rech, and M. Ghioni, "Complete and compact 32-channel system for time-correlated single-photon counting measurements," IEEE Photonics J. **5**, 6801514 (2013).
[20]R. A. Colyer, G. Scalia, F. Villa, F. Guerrieri, S. Tisa, F. Zappa, S. Cova, S. Weiss, and X. Michalet, "Ultra high-throughput single molecule spectroscopy with a 1024 pixel SPAD," Proc. SPIE **7905**, 790503 (2011).
[21]X. Michalet, R. A. Colyer, G. Scalia, A. Ingargiola, R. Lin, J. E. Millaud, S. Weiss, O. H. W. Siegmund, A. S. Tremsin, J. V. Vallerga, A. Cheng, M. Levi, D. Aharoni, K. Arisaka, F. Villa, F. Guerrieri, F. Panzeri, I. Rech, A. Gulinatti, F. Zappa, M. Ghioni, and S. Cova,"Development of new photon-counting detectors for single-molecule fluorescence microscopy," Philos. Trans. R. Soc., B **368**, 20120035 (2012).
[22]M. Kloster-Landsberg, D. Tyndall, I. Wang, R. Walker, J. Richardson, R. Henderson, and A. Delon, "Note: Multi-confocal fluorescence correlation spectroscopy in living cells using a complementary metal oxide semiconductor-single photon avalanche diode array," Rev. Sci. Instrum. **84**, 076105 (2013).
[23]L. Carrara, C. Niclass, N. Scheidegger, H. Shea, and E. Charbon, "A gamma, X-ray and high energy proton radiation-tolerant CMOS image sensor for space applications," *IEEE International Solid-State Circuits Conference* (IEEE, 2009), pp. 40–41.
[24]J. Huisken, J. Swoger, F. Del Bene, J. Wittbrod, and E. H. K. Stelzer, "Optical sectioning deep inside live embryos by selective plane illumination microscopy," Science, **305**(5686), 1007–1009 (2004).
[25]A. Singh, J. Krieger, J. Buchholz, E. Charbon, J. Langowski, and T. Wohland, "The performance of 2D array detectors for light sheet based fluorescence correlation spectroscopy," Opt. Express **21**, 8652–8668 (2013).
[26]I. Rech, S. Marangoni, D. Resnati, M. Ghioni, and S. Cova, "Multipixel single-photon avalanche diode array for parallel photon counting applications," J. Mod. Opt. **56**, 326–333 (2009).
[27]A. Gulinatti, I. Rech, P. Maccagnani, S. Cova, and M. Ghioni, "New silicon technologies enable high-performance arrays of single photon avalanche diodes," Proc. SPIE **8727**, 87270M (2013).
[28]M. Zhao, L. Jin, B. Chen, Y. Ding, H. Ma, and D. Chen, "Afterpulsing and its correction in fluorescence correlation spectroscopy experiments," Appl. Opt. **42**, 4031–4036 (2003).
[29]J. Enderlein and I. Gregor, "Using fluorescence lifetime for discriminating detector afterpulsing in fluorescence-correlation spectroscopy," Rev. Sci. Instrum. **76**, 033102 (2005).
[30]OptoSplit II LS Image Splitter, application note, Cairn Research, 2014, available online at: http://www.cairn-research.co.uk/sites/default/files/products/datasheets/OptoSplit%20II%20LS%20ds%2006-14.pdf.
[31]A. Ingargiola, R. A. Colyer, D. Kim, F. Panzeri, R. Lin, A. Gulinatti *et al.*, "Parallel multispot smFRET analysis using an 8-pixel SPAD array," in Proc. SPIE **8228**, 82280B (2012).
[32]A. Lacaita, F. Zappa, S. Bigliardi, and M. Manfredi, "On the bremsstrahlung origin of hot-carrier-induced photons in silicon devices," IEEE Trans. Electron. Dev. **40**, 577–582 (1993).
[33]K. Schatzel, M. Drewel, and S. Stimac, "Photon correlation measurements at large lag times: improving statistical accuracy," J. Mod. Opt. **35**, 711–718 (1988).
[34]Z. Kojro, "Normalization and statistical noise level in the normalized autocorrelation function. Compensated nomalization," J. Phys. A: Math. Gen. **24**, L225–L229 (1991).
[35]K. Schatzel, "Noise on photon correlation data - I. Autocorrelation functions," Quantum Opt. **2**, 287–305 (1990).
[36]D. Magatti and F. Ferri, "Fast multi-tau real-time software correlator for dynamic light scattering" Appl. Opt. **40**, 4011–4021 (2001).
[37]S. Gong, I. Labanca, I. Rech, and M. Ghioni, "A simple and flexible FPGA based autocorrelator for afterpulse characterization of single-photon detectors," in *11th International Multi-Conference on Systems, Signals and Devices (SSD)* (IEEE, 2014), pp. 1–6.
[38]See http://www.xilinx.com/publications/prod_mktg/Spartan6_Product_Table.pdf for Spartan 6 Product Table, Xilinx Inc.
[39]A. Lacaita, M. Ghioni, and S. Cova, "Double epitaxy improves single-photon avalanche diode performance," Electron. Lett. **25**, 841–843 (1989).
[40]D. T. Fewer, S. J. Hewlett, E. M. McCabe, and J. Hegarty, "Direct-view microscopy: experimental investigation of the dependence of the optical sectioning characteristics on pinhole-array configuration," J. Microsc. **187**, 54–61 (1997).
[41]S. Cova, M. Ghioni, A. Lacaita, C. Samori, and F. Zappa, "Avalanche photodiodes and quenching circuits for single-photon detection," Appl. Opt. **35**, 1956–1976 (1996).
[42]S. M. Sze, *Physics of Semiconductor Devices* (Wiley, New York, 1981), pp. 520–527.
[43]G. A. M. Hurkx, H. C. de Graaff, W. J. Kloosterman, and M. P. G. Knuvers, "A new analytical diode model including tunneling and avalanche breakdown," IEEE Trans. Electron Devices **39**, 2090–2098 (1992).
[44]S. Cova, A. Lacaita and G. Ripamonti, "Trapping phenomena in avalanche photodiodes on nanosecond scale," IEEE Electron. Device Lett. **12**, 685–687 (1991).
[45]I. Rech, A. Ingargiola, R. Spinelli, I. Labanca, S. Marangoni, M. Ghioni, and S. Cova, "A new approach to optical crosstalk modeling in single-photon avalanche diodes," IEEE Photon. Technol. Lett. **20**, 330–332 (2008).
[46]I. Rech, A. Ingargiola, R. Spinelli, I. Labanca, S. Marangoni, M. Ghioni, and S. Cova, "Optical crosstalk in single photon avalanche diode arrays: a new complete model," Opt. Express **16**, 8381–8394 (2008).
[47]A. Cuccato, "Development of electronic systems for single-photon avalanche diode arrays," Ph.D. thesis (Politecnico di Milano, 2013).
[48]P. Schwille, F. J. Meyer-Almes, and R. Rigler "Dual-color fluorescence cross-correlation spectroscopy for multicomponent diffusional analysis in solution," Biophys. J. **72**, 1878–1886 (1997).

This article is copyrighted as indicated in the article. Reuse of AIP content is subject to the terms at: http://scitationnew.aip.org/termsconditions. Downloaded to IP: 131.175.132.142 On: Fri, 03 Oct 2014 14:36:06